SUPPORTING INFORMATION

Ultra Sensitive Detection of Leukemia by Graphene

Figure S1a and Figure S2A present typical AFM images of the GONPs (used in the guanine extraction) and GO sheets (applied in fabrication of the rGONW electrodes) on the Si(100) substrates, respectively. The GONPs with lateral dimensions of ~20–200 nm and knife-like edges are clearly observable in Figure S1a. The GO sheets with lateral dimensions ~1 μm are also distinguishable in Figure S2A. The height profile distributions of the nanoplatelets and sheets are also shown in Figure S1b and Figure S2B. It is well-known that typical thicknesses of monolayer (ML) GO is ~0.8 nm, *i.e.* ~0.44 nm thicker than the thickness of graphene (~0.36 nm), because of the presence of the oxygen bonds on the both sides.[1–3] In each height profile distribution, the minimum fluctuations which are related to the roughness of the background surface were set to zero. Hence, the first peaks after the fluctuations (here, located at ~0.8 nm) can be assigned to the thickness of single-layer GO deposited on the Si substrate. The next peaks located at ~1.6 and 2.4 nm can be attributed to the double- and triplet-layer GO. These results indicate that the graphene nanoplatelets and sheets composed of ≤2 and 4 layers, respectively.

Figure S2C–E show scanning electron microscope (SEM) images of the rGONWs deposited on surface of a graphite electrode by EPD. A nest-like porous nanostructure constructed by graphene nanowalls with ultra sharp edges (<10 nm edge thicknesses), lateral dimensions of ~100–500 nm, and nearly vertical orientations with respect to the substrate are seen. Such porous graphene electrodes would provide unique electrochemical properties, because of their large surface area and excellent capability in charge transferring through the ultra sharp edges of the vertical nanowalls.

Raman spectroscopy was utilized to investigate about the carbon structure of the GONPs and rGONW electrodes. The famous bands of carbon in Raman spectra, *i.e.*, the G band (~1585 cm^{-1})

resulted from the first-order scattering of the E_2g phonons of graphitic structure of carbon and the D band (~1350 cm^{-1}) resulted from a breathing mode of κ-point phonons of A_1g symmetry of structural defects induced by, e.g., hyrodxyl and/or epoxide bonds [4], are seen in Figure S1c and Figure S2F. The I_G/I_D ratio, which is a measure of the sp^2 domain size in a carbon structure containing sp^3 and sp^2 bonds, was found 0.74 for the GONPs, 1.37 for the GONW and 1.11 for the rGONW electrodes. The lower I_G/I_D ratio of the GONPs than the typical ratio for the GO sheets (~0.85)[5] can be attributed to the smaller lateral dimension of the former resulting in higher edge defects. For the graphene nanowall electrodes, although the edge defects/disorders of the nanowalls would result in low I_G/I_D ratios (with values < 1), [6] the I_G/I_D ratios > 1 were assigned to graphitic structure of the substrate, consistent with our previous report. [7]

Raman spectroscopy is also known as an effective technique to discriminate the single- and multi-layer characteristics of graphene, because the 2D band is highly sensitive to the layer stacking.[8] For example, single-layer graphene present a 2D band at 2679 cm^{-1}, whilst the 2D band of multi-layer graphene (including 2–4 layers) appears as a widened peak at higher wavenumbers (by 19 cm^{-1}).[9] In addition, the typical I_{2D}/I_G intensity ratio of single-, double-, triple- and multi- (>4) layer graphene is >1.6, ~0.8, ~0.30 and ~0.07, respectively (see, e.g., [10–1112]). In this work, the I_{2D}/I_G intensity ratio of GONPs was found ~0.47. This reconfirmed the single- and double-layer structure of GONPs (consistent with the results of the AFM analysis).

Figure S1d and Figure S2G show peak deconvolution of C(1s) core level of XPS of the GONPs and graphene nanowall electrodes (the GONW and rGONW electrodes), respectively. In the peak deconvolution, the peaks located at 285.0 eV was assigned to the C–C and C=C bonds. The other deconvoluted peaks located at the binding energies of 286.5, 287.2, 288.3 and 289.4 eV were attributed to the C–OH, C–O–C, C=O, and O=C–OH oxygen-containing functional groups, respectively (see, for example, [13,14]). The sample reduced by hydrazine (the rGONW electrode) shows another peak component at 285.9 eV which can be attributed to formation of C–N bonds.[15] Based on the XPS analysis, it was found that reduction pf the GONWs into the rGONWs resulted in decreasing the O/C

atomic ratio from 0.44 to 0.17, indicating substantial deoxygenation of the GONWs (~60%) under the reduction condition.

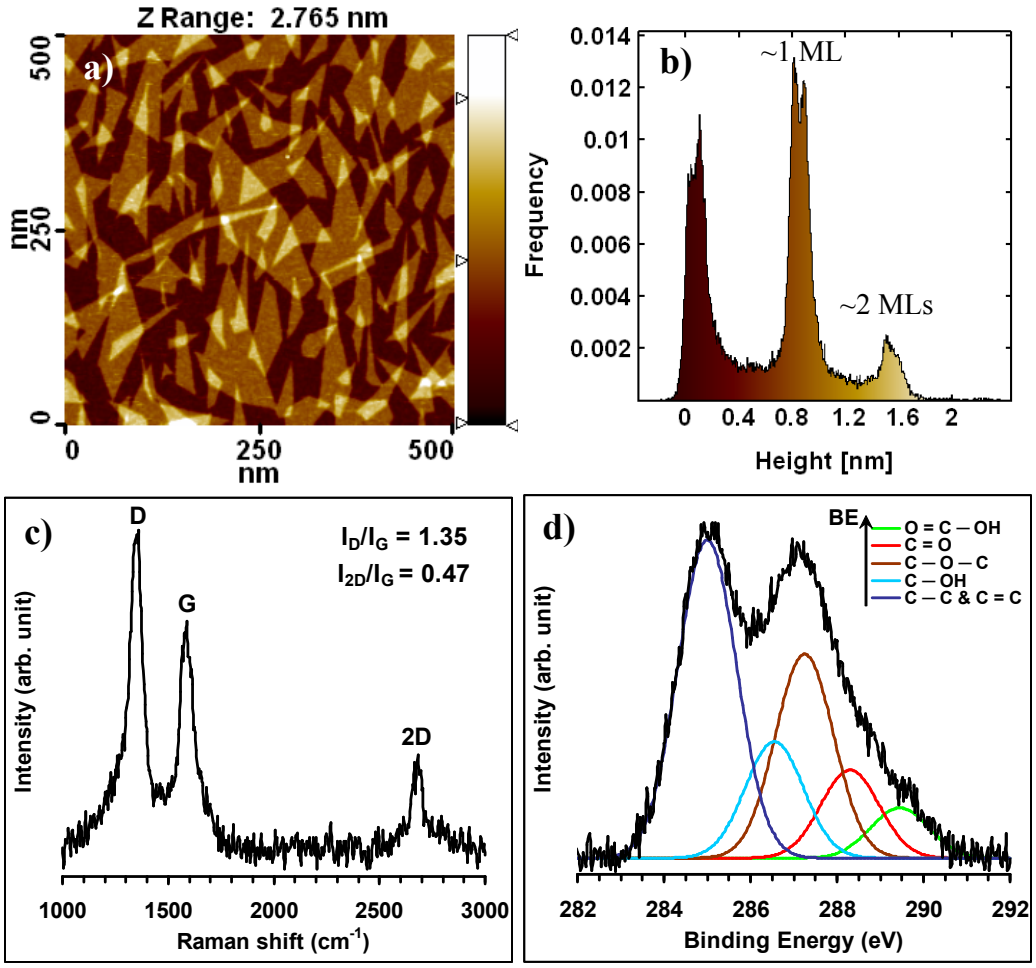

Figure S1. a) AFM image, b) height profile distribution, c) Raman spectrum and d) XPS of GONPs.

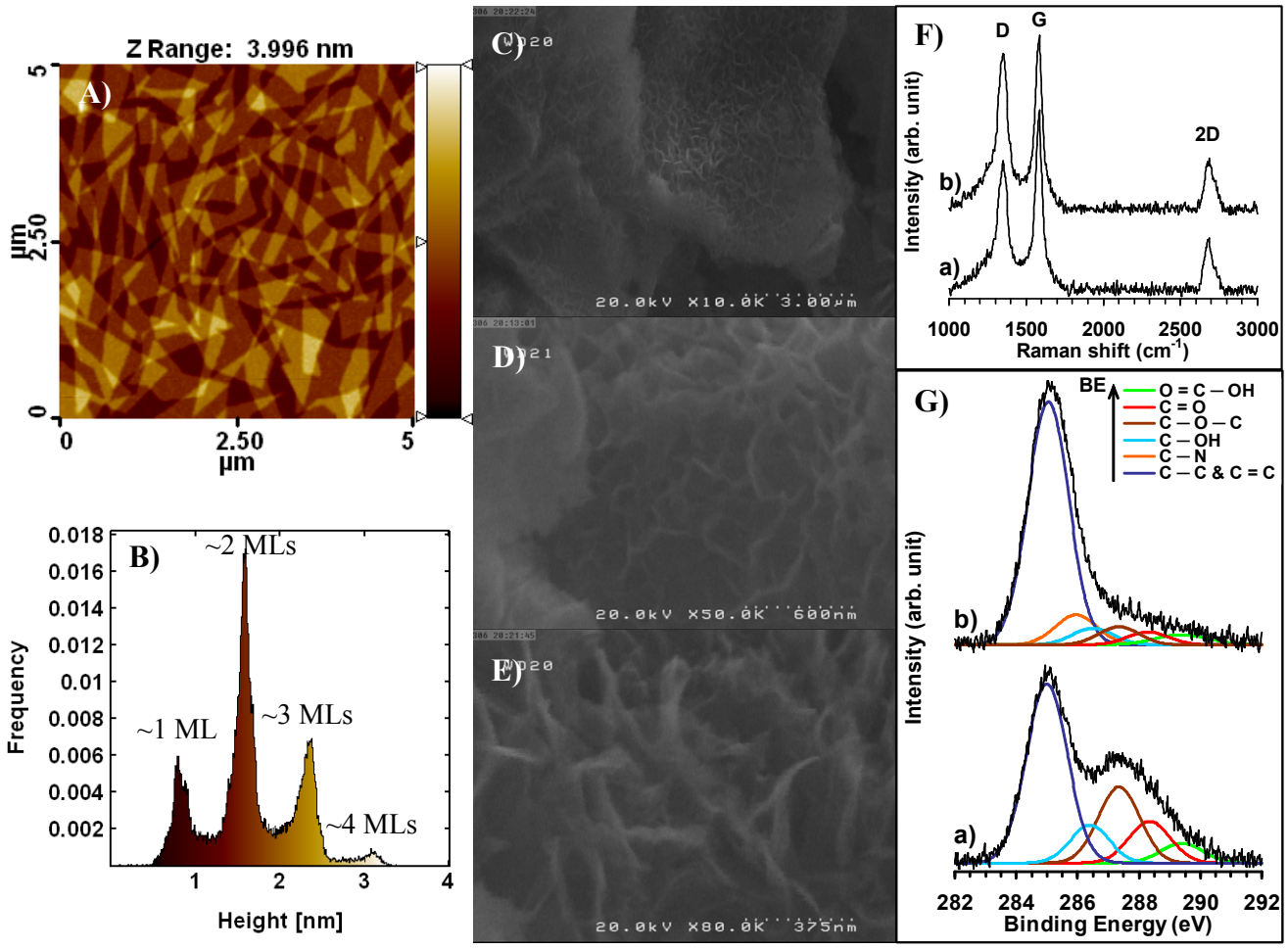

Figure S2. A) AFM image and B) height profile distribution of GO sheets used in the EPD, SEM images of rGONWs deposited on a graphite rod in various magnifications: a) 10,000 (a wide windo with scale bar of 3 µm), b) 50,000 (a closed up widow with scale bar of 600 nm) and c) 80,000 (a tilted situation with scale bar of 375 nm), F) Raman spectra and h) deconvoluted C(1s) core level of XPS of a) GONW and b) rGONW electrodes.

RERERENCES AND NOTES

[1]Schniepp, H. C.; Li, J. L.; McAllister, M. J.; Sai, H.; Herrera-Alonso, M.; Adamson, D. H.; Prud'homme, R. K.; Car, R.; Saville, D. A.; Aksay, I. A. Functionalized Single Graphene Sheets Derived from Splitting Graphite Oxide. *J. Phys. Chem. B* **2006**, *110*, 8535–8539.

[2]Mc Allister, M. J.; Li, J. L.; Adamson, D. H,; Schniepp, H. C.; Abdala, A. A.; Liu, J.; Herrera-Alonso, M.; Milius, D. L.; Car, R.; Prud'homme, R. K.; Aksay I. A. Single Sheet Functionalized Graphene by Oxidation and Thermal Expansion of Graphite. *Chem. Mater.* **2007**, *19*, 4396–4404.

[3]Akhavan, O. The Effect of Heat Treatment on Formation of Graphene Thin Films from Graphene Oxide Nanosheets. *Carbon* **2010**, *48*, 509–519.

[4]Ferrari, A. C.; Robertson, J. Interpretation of Raman Spectra of Disordered and Amorphous Carbon. *Phys. Rev. B* **2000**, *61*, 14095–14107.

[5]Akhavan, O.; Abdolahad, M.; Esfandiar, A.; Mohatashamifar, M. Photodegradation of Graphene Oxide Sheets by TiO_2 Nanoparticles after a Photocatalytic Reduction. *J. Phys. Chem. C* **2010**, *114*, 12955–12959.

[6]Akhavan, O.; Ghaderi, E. Toxicity of Graphene and Graphene Oxide Nanowalls Against Bacteria. *ACS Nano* **2010**, *4*, 5731–5736.

[7]Akhavan, O.; Ghaderi, E.; Rahighi, R. Toward Single-DNA Electrochemical Biosensing by Graphene Nanowalls. ACS Nano **2012**, *6*, 2904–2916.

[8]Malard, L. M,; Pimenta, M. A.; Dresselhaus, G.; Dresselhaus, M. S. Raman Spectroscopy in Graphene. *Phys. Rep.* **2009**, *473*, 51–87.

[9]Graf, D.; Molitor, F.; Ensslin, K.; Stampfer, C.; Jungen, A.; Hierold, C.; Wirtz, L. Spatially Resolved Raman Spectroscopy of Single- and Few-Layer Graphene. *Nano Lett.* **2007**, *7*, 238–242.

[10]Kim, K.S.; Zhao, Y.; Jang, H.; Lee, S. Y.; Kim, J. M.; Kim, K. S.; Ahn, J. H.; Kim, P.; Choi, J.Y.; Hong, B. H. Large-Scale Pattern Growth of Graphene Films for Stretchable Transparent Electrodes.

Nature **2009**, *457*, 706–710.

[11]Calizo, I.; Balandin, A. A.; Bao, W.; Miao, F.; Lau, C. N. Temperature Dependence of the Raman Spectra of Graphene and Graphene Multilayers. *Nano Lett.* **2007**, *7*, 2645–2649.

[12]Liu, L.; Ryu, S.; Tomasik, M. R.; Stolyarova, E.; Jung, N.; Hybertsen, M. S.; Steigerwald, M. L.; Brus, L. E.; Flynn, G. W. Graphene Oxidation: Thickness-Dependent Etching and Strong Chemical Doping. *Nano Lett.* **2008**, *8*:1965–1970.

[13]Liu, F.; Seo, T. S. A Controllable Self-Assembly Method for Large-Scale Synthesis of Graphene Sponges and Free-Standing Graphene Films. *Adv. Funct. Mater.* **2010**, *20*, 1930–1936.

[14]Akhavan, O.; Kalaee, M.; Alavi, Z. S.; Ghiasi, S. M. A.; Esfandiar, A. Increasing the Antioxidant Activity of Green Tea Polyphenols in the Presence of Iron for the Reduction of Graphene Oxide. *Carbon* **2012**, *50*:3015–3025.

[15]Esfandiar, A.; Akhavan, O.; Irajizad, A. Melatonin as a Powerful Bio-antioxidant for Reduction of Graphene Oxide. *J. Mater. Chem.* **2011**, *21*, 10907–14.